Dong Wang, Lanying Lin*, Feng Fu, and Mizi Fan

Fracture mechanisms of softwood under longitudinal tensile load at the cell wall scale

https://doi.org/10.1515/hf-2019-0112
Received April 18, 2019; accepted November 5, 2019; previously published online xx

Abstract: This study was undertaken to elucidate the longitudinal tensile fracture behaviors of softwood at the cell wall scale by means of microscopic analyses. The fracture types of the tracheids at the different fracture surfaces were also distinguished. The results indicated that the main tracheid fracture of the earlywood (EW) sample was transverse transwall breakage. The tracheid fracture process of the transverse transwall breakage was initiated as a fracture in the S_2 layer, with the crack propagating into the S_1/S_2 interface. For the EW/latewood (LW) sample, the strain concentration and initial crack under longitudinal tensile load generally occurred in wood rays in the EW part, which caused the tracheids to experience transverse transwall breakage. The differences in longitudinal and transverse strains between EW and LW under longitudinal tensile load led to shear stress and parallel-to-grain cracks occurring at the growth ring border. When the crack propagated along the wood grain in the EW tissue or growth ring boundary, this resulted in EW longitudinal transwall breakage. However, when the crack propagates along the wood grain in the LW tissue, it could cause the LW tracheid to undergo intrawall breakage, with the crack occurring predominantly at the compound middle lamella (CML)/S_1 interface region.

Keywords: crack propagation, fracture initiation, longitudinal tensile load, softwood

***Corresponding author: Lanying Lin,** Research Institute of Wood Industry, Chinese Academy of Forestry, Beijing 100091, China; and College of Engineering, Design and Physical Sciences, Brunel University, Middlesex UB8 3PH, UK, e-mail: linly@caf.ac.cn
Dong Wang: Nanjing Forestry University of Materials and Science and Engineering, Nanjing 210037, China; and Research Institute of Wood Industry, Chinese Academy of Forestry, Beijing 100091, China
Feng Fu: Research Institute of Wood Industry, Chinese Academy of Forestry, Beijing 100091, China
Mizi Fan: College of Engineering, Design and Physical Sciences, Brunel University, Middlesex UB8 3PH, UK

Introduction

Wood is a complex, heterogeneous and anisotropic material composed of cells varying in size, orientation and wall structure depending on the function they perform in the tree (Smith and Vasic 2003). This complex structure makes the fracture of wood more complicated compared to more homogeneous materials. A better understanding of the fracture mechanisms of wood structures may allow the more efficient use and better utilization of wood and wood composites.

In general, fractures in wood are induced by growth structure differences, which cause localized stress peaks (Lukacevic et al. 2015). Furthermore, growth defects, such as knots, a diagonal grain, intercellular spaces and pits, are known to play an important role in the behavior of wood fractures (Akande and Kyanka 1990; Zink et al. 1994; Mott et al. 1995). The influence of wood structure on fracture initiation and crack growth behavior under longitudinal tensile load has long been considered to be of great importance (Mark 1967). Wood rays have been shown to serve as structural points of weakness, and the longitudinal tension-induced fracture initiation at the specimen surface has always been associated with perpendicular-to-grain cracks in wood rays (Bodner et al. 1996, 1997). Furthermore, the differences in mechanical properties between the earlywood (EW) and latewood (LW) can lead to parallel-to-grain cracks occurring at the EW/LW borders (Sippola and Frühmann 2002). Those differences in mechanical properties were determined mainly via investigation of separated EW and LW fibers or sections (Sinn et al. 2001; Cramer et al. 2005; Lanvermann et al. 2014; Büyüksari et al. 2017), but the interaction influences of EW and LW on the wood fracture have been neglected. As such, the importance of the scale interaction and combined influences of microstructures and stress/strain must also be emphasized (Davies 1968; Sippola and Frühmann 2002; Stanzl-Tschegg and Navi 2009). Finally, the resin ducts, presenting larger voids, also affect wood fracture initiation and crack growth behaviors (Bodner et al. 1998). Although crack initiation and propagation within the wood macrostructure have been well understood, very few attempts have been made to investigate crack initiation and growth modes along with the fracture mechanisms at a cellular level.

Fractures have to proceed through the cells, and therefore, the degree of deformation and location of the cell wall plays an important role in characterizing the fracturing of wood. At the scale of individual cells, four types of cell fractures are recognized: intercell, the separation of cells at the middle lamella (ML) (Koran 1968; Cote and Hanna 1983; Zink et al. 1994); intrawall, within the secondary cell wall (Cote and Hanna 1983; Zink et al. 1994); transverse transwall, across the cell walls and perpendicular to the grain; and longitudinal transwall, across the cell walls but parallel to the grain, where the cell lumen is exposed (Zink et al. 1994). Cell wall fracturing, as well as propagation under longitudinal tensile load, was reviewed by Mark (1967), and this study concluded that initiation of fractures occurred in the secondary wall S_1 layer or the S_1/S_2 interface, rather than in the ML layer. However, previous results have also shown that, when wood is subjected to a longitudinal tensile stress, cracks in the cell walls occur in the S_2 layer (Fahlén and Salmén, 2002). Therefore, it is evident that the initial crack and crack propagation in the cell wall is not completely understood. Furthermore, the cell fracture types of the different fracture surfaces owing to crack initiation and propagation in different tissues also need to be distinguished.

The primary focuses of this investigation were to distinguish the tracheid fracture types of the different fracture surfaces, and to analyze the mechanisms of crack initiation and propagation at the cell wall scale. Furthermore, other aspects of the presented work were to investigate the effects of wood ray as well as interaction between EW and LW on softwood tensile fracturing and tracheid breakage type.

Materials and methods

Materials: The two species of wood materials were sampled from Masson pine (*Pinus massoniana* Lamb., basic density = 0.51 g cm^{-3}) and Norway spruce (*Picea asperata* Mast., basic density = 0.42 g cm^{-3}), with the Norway spruce representing a typical softwood and the Masson pine being one of the major softwoods in China. The samples were prepared from heights of 1.5 m ~ 2.0 m. The longitudinal/radial sections (8 ~ 10 growth rings in width) of the specimens are presented in Figure 1a. All of the tensile specimens were cut into dumbbell-type shapes, as shown in Figure 1a. The goal of this design was to achieve a larger gripping area to avoid the possibility of slippage in the tensile testing grip and preventing stress concentration at the grips, forcing fractures to occur in the constricted neck area. The specimens were oriented in the crack propagation system. For reference, R = radial, T = tangential and L = longitudinal, where the first letter indicates the load direction, and the second determines the direction of crack propagation. Prior to testing, all specimens were conditioned in a desiccator (NaCl saturated salt solution, 25°C) for 12 weeks, and the resulting average moisture content of all the specimens was 13.4%.

Methods

Tensile testing on small clear specimens

Tensile tests were performed in the wood grain direction: a tensile tester (Instron 5848 Crop, Instron, Norwood, MA, USA) equipped with a load cell with a capacity of 2 kN was applied (displacement rate 0.15 mm min^{-1}). The thickness of the small clear specimens for tensile testing was 1 mm, and the constricted neck areas of 2 × 30 mm^2 (R × L) were present as EW or an EW/LW combination (Figure 1a). Fifteen specimens of EW or EW/LW were tested. After the mechanical tests, the fracture surfaces of the two tested specimens, representing the EW or EW/LW of each species, were observed in detail via field-emission scanning electron microscopy (ESEM) and atomic force microscopy (AFM) to examine softwood and tracheid fracture behaviors.

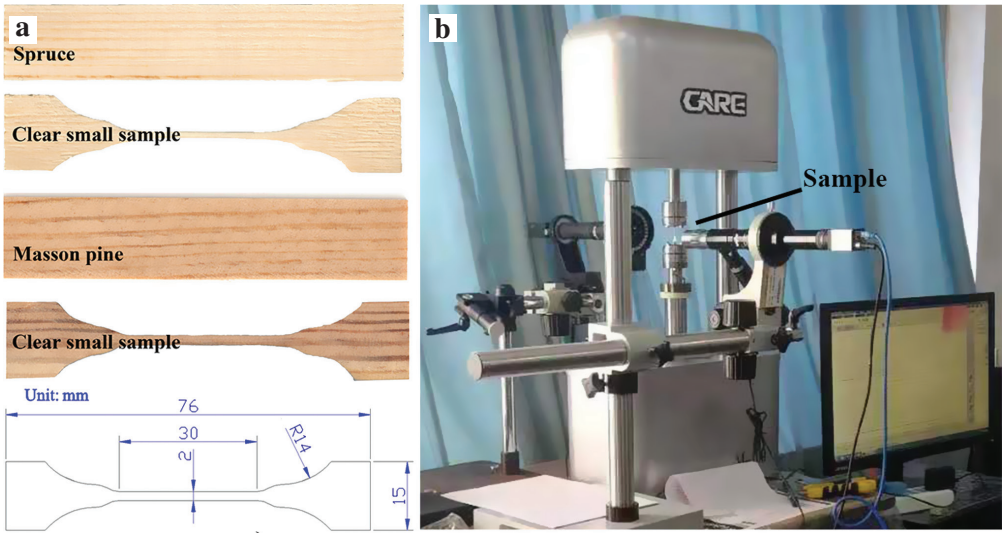

Figure 1: Samples preparation and DSCM test system.
(a) Small clear samples of the spruce or Masson pine; (b) DSCM test system.

ESEM and AFM imaging

Detailed longitudinal tensile fracture surface characteristics of the small clear specimens were observed with a Hitachi S-4800 ESEM (Hitachi, Tokyo, Japan) after sputter coating the samples with gold in a vacuum chamber. The tracheid cross-section features of the fracture surfaces were examined in detail at the cellular scale using high-resolution AFM (Veeco, Plainview, NY, USA). Standard tapping mode probes (Bruker, RTESP-300, Blerika, MA, USA) were used. The length of the cantilever was 125 μm, and the resonance frequency was 300 kHz. Prior to AFM testing, the broken part of the small clear tensile specimen was embedded in resin. The embedding resin consisted of SPI-PON812 resin, hardener [dodecenyl succinic anhydride (DDSA)], plasticizer [nadic methyl anhydride (NMA)] and curing agent [Tris-(dimethyl amino methyl) phenol (DMP-30)] (Structure Probe, Inc., West Chester, PA, USA). The specimens were first vacuum impregnated (−0.1 MPa for 30 min) and then pressure impregnated (1.0 MPa for 8 h) to ensure that both the cell lumens and cell wall cracks were fully impregnated. This method was able to distinguish between cell wall tensile fracture cracks and cracks caused by subsequent AFM sample preparation; the former cracks were filled with resin, but the latter were not. Secondly, a freshly cut surface was made using an ultramicrotome (Leica EM UC7, Wetzlar, Germany), and the cross-section morphology was then assessed using AFM. For obtaining detailed crack information regarding fracture initiation and crack growth at individual cell walls, the fracture morphologies of the cell wall cross-sections were scanned via AFM for every 100 μm from the top of the fracture section to the end.

The digital speckle correlation method (DSCM)

The image capturing system for DSCM is depicted in Figure 1b, and the effects of strain differences between EW and LW as well as wood rays on wood deformation were monitored by tracking the displacement of markers on the specimen surface. The dynamic tensile processes of the specimens during longitudinal tensile testing were recorded using a high-speed Basler charge coupled device (CCD) video camera at three frames per second. The displacement rate was 0.15 mm min^{-1}, and the load-displacement curves were recorded simultaneously. Over a hundred images were captured, which were paired and analyzed to acquire the tensile-strain fields. To obtain excellent stochastic black for the DSCM, the specimen surfaces were sprayed with black carbon ink. A rectangular region of 2 mm × 2.5 mm was defined on each initial image of the specimen. The thicknesses of the small clear specimens for DSCM testing were designated at 0.5 mm due to the limitation of the maximum load capacity (200N) of the mechanical testing device in combination with DSCM, but the other geometric parameters of the specimens were the same as the tensile fracture testing specimens (Figure 1a).

Results and discussion

Tensile fractures of the small clear samples

The EW samples' longitudinal tensile fractures

Representative load-displacement curves are presented in Figure 2, where the brittle ruptures of all the specimens

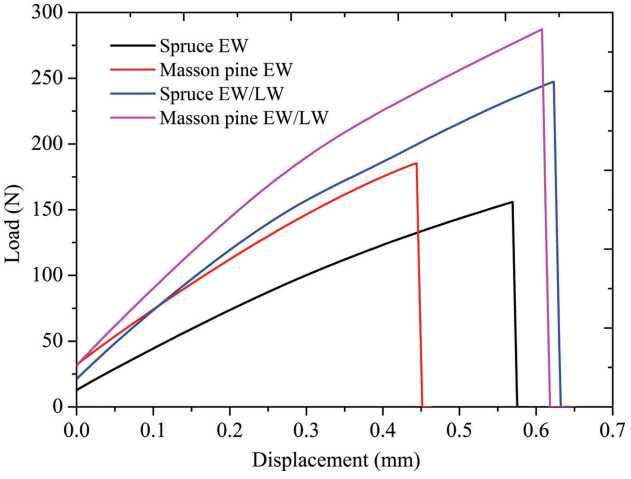

Figure 2: Longitudinal tensile load-displacement curves of the spruce and Masson pine specimens.

are clearly seen. The fracture surface of the small clear EW specimen and the tracheid breakage types for the spruce and Masson pine under longitudinal tensile load are shown in Figures 3 and 4. The longitudinal-radial (LR) fracture surface of the spruce EW sample was relatively flat and perpendicular to the wood longitudinal direction (Figure 3a). The breakage type of the tracheids was transverse transwall (Figure 3b). There were many cracks in the cell wall S_2 layer, and interfacial debonding also occurred in the S_1/S_2 layer (Figure 3b). The detailed cracks of the cross-section of the breakage tracheids are illustrated in the AFM images. There were two kinds of cracks in the tracheid cross-section, including trumpet-shaped cracks in the S_2 layer and S_1/S_2 interface debonding (Figure 4c). Based on the direction of the trumpet-shaped crack tip, the tracheid wall fracture process was speculated to have initiated via a fracture occurring in the S_2 layer, and the crack was then propagated into the S_1/S_2 interface (Figure 3d,e).

For the EW of the Masson pine specimen, one of the most apparent characteristics of the fracture surface was that it had many cell wall fragments (Figure 4a), and a part of the front surface of the visible ray had peeled off. The crack propagation along the wood ray length direction resulted in tracheids near the wood rays incurring transverse transwall breakage. The LR fracture surface of region I in Figure 3 was relatively flat and perpendicular to the wood longitudinal direction. Figure 4b–g depict AFM images of the tension-induced cell wall cross-section fracture morphologies of the different fracture regions. The breakage type of the tracheids in region I (Figure 3a) was transverse transwall and is schematized in Figure 4f. Figure 4g depicts an enlarged version of the section within the dashed lines in Figure 4f. The initial crack also

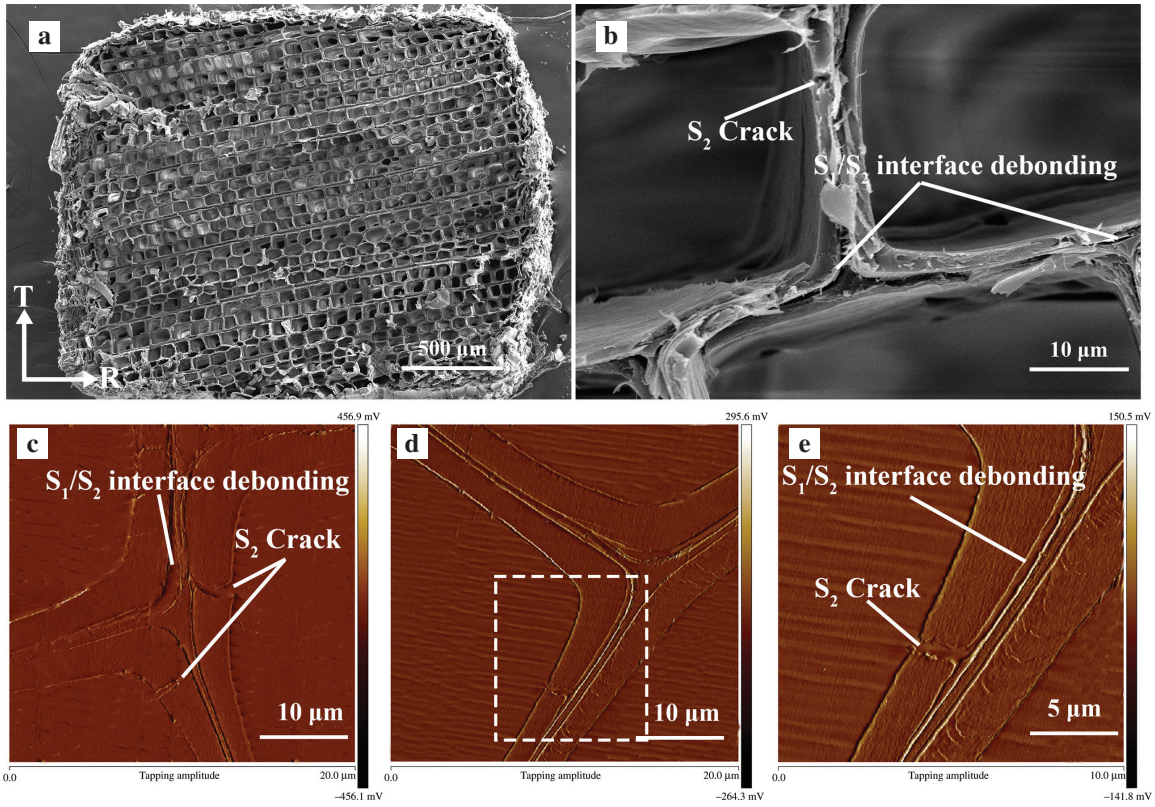

Figure 3: The fracture surface and tracheid cross-sections indicating the fracture morphologies of the spruce EW.
(a and b) SEM images of the LR fracture surface; (a and d) AMF images of the tracheid cross-sections indicating the fracture morphologies; (e) an enlarged version of the section within the dashed lines in (d).

occurred in the S_2 layer and propagated into the S_1/S_2 interface (Figure 4f).

For the tracheids between two adjacent rows of wood rays (region II in Figure 4a), the main fracture type was also transverse transwall breakage, but the fracture surface was not completely perpendicular to the wood longitudinal direction, and parts of the cell lumens were exposed. In the II to IV regions, more and more cell lumens were exposed (Figure 4a). The main reason for this occurrence was that a shear stress perpendicular to the LR fracture surface of region I (Figure 4) would be generated, and this forced the crack to propagate along the longitudinal direction. Moreover, the roughly fractured surfaces from the regions II to IV revealed a tendency to form a spiral arrangement of some layers within the tracheid walls. At the scale of individual cells, the initial crack and crack propagation of the tracheid walls for regions II and III were similar to that of region I (Figure 3b,d); however, the fracture type of the tracheids in region IV was longitudinal transwall, owing to crack propagation along the longitudinal direction (Figure 4e).

According to the above observations, the fracture morphology analyses of the EWs from both species indicated that the fracture surface of the Masson pine specimen was relatively complex compared with the fracture surface morphology of the spruce EW specimen. One possible reason for this occurrence was that more wood rays in the Masson pine resulted in the crack propagation becoming more complex. However, at the cell wall scale, the initial crack of the tension-induced transverse transwall of the tracheids in the two species all occurred in the S_2 layer, and the crack then propagated into the S_1/S_2 interface. Furthermore, our results detailing that tracheid transverse transwall breakage were not consistent with those of Mark (1967), who reviewed previous studies indicating that the initial tension-induced fracture typically occurred at the S_1/S_2 interface.

The EW/LW samples' longitudinal tensile fractures

Figures 5 and 6 illustrate the fracture surfaces and cell wall cross-section fracture morphologies under a longitudinal tensile load of the small clear EW/LW combination Masson pine and spruce samples. In all specimens, the fracture progressed in a stepwise manner. The fractures

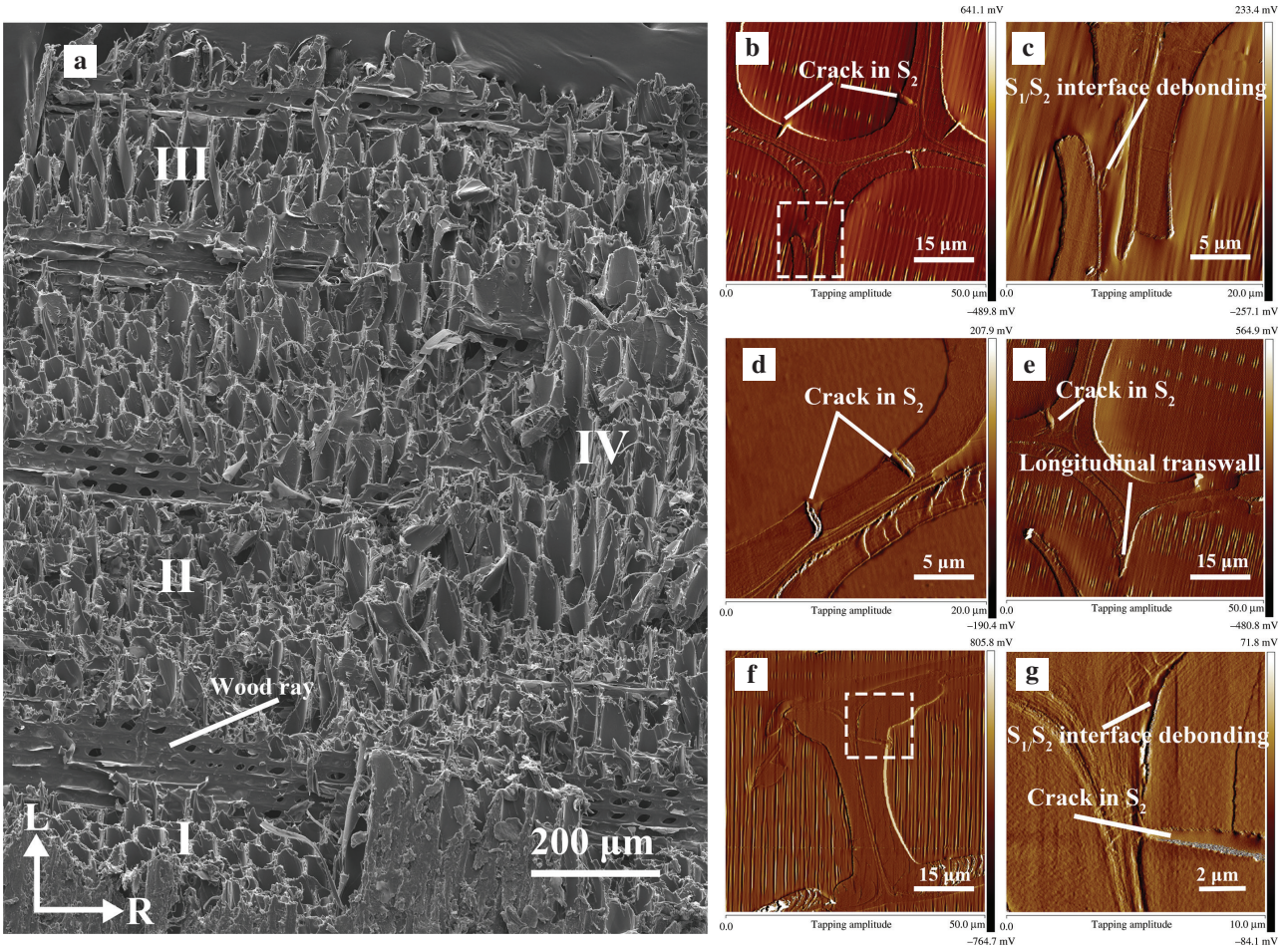

Figure 4: The fracture surface and tracheid cross-sections indicating the fracture morphologies of Masson pine EW.
(a) SEM image of the fracture surface; (b, d and e) AMF images of tracheid cross-sections of the fracture regions I, II and III in Figure 4a, respectively; (c and g) enlarged versions of the sections within the dashed lines in b and f, respectively.

showed splintering fracture modes, which were mainly due to cracks parallel to the grain along the growth ring borders. Separation of cells along the growth ring borders was frequent in the Masson pine and spruce samples with well-defined growth rings (Figures 5 and 6). The cracks propagated along the radial direction and formed an LR fracture surface in the EW tissue of the spruce or Masson pine EW/LW combination specimens (region I in Figures 5a and 6a). The breakage type of the tracheids in this fracture surface was transverse transwall. Figures 5b and 6b present AFM images depicting the cross-sections of the LR fracture surfaces. Figures 5c and 6c are an enlarged version of the section within the dashed lines in Figures 5b and 6b, respectively. There were two kinds of cracks in the tracheid wall cross-sections, including through cracks in the S_2 layer and S_1/S_2 interface debonding (Figures 5c and 6c). The cracks propagated across the EW tissues until they reached the dense LW, which blocked further crack growth. Accordingly, the crack deviated from the initial direction and propagated through the relatively weak interfacial areas between the EW and LW. A new fracture surface was formed in the EW near the growth ring (region III in Figures 5a and 6a). When the crack propagated along the wood grain in the EW tissue or growth ring boundary, this resulted in EW longitudinal transwall breakage (Figures 5e and 6e). The crack propagating along the wood grain in the LW tissue could cause the LW tracheid to undergo intrawall breakage, with the crack occurring predominantly at the compound middle lamella (CML)/S_1 interface region (Figures 5d and 6d).

However, there were also differences in the fracture surface morphologies between the spruce and Masson pine specimens. The EW fracture surface near the growth ring of the spruce specimen was quite clear, with many fragments generated from the crack propagation (Figure 5a,e). However, the EW fracture surface near the growth ring of the Masson pine presented visible cell lumens whose surfaces were totally smooth (Figure 6a).

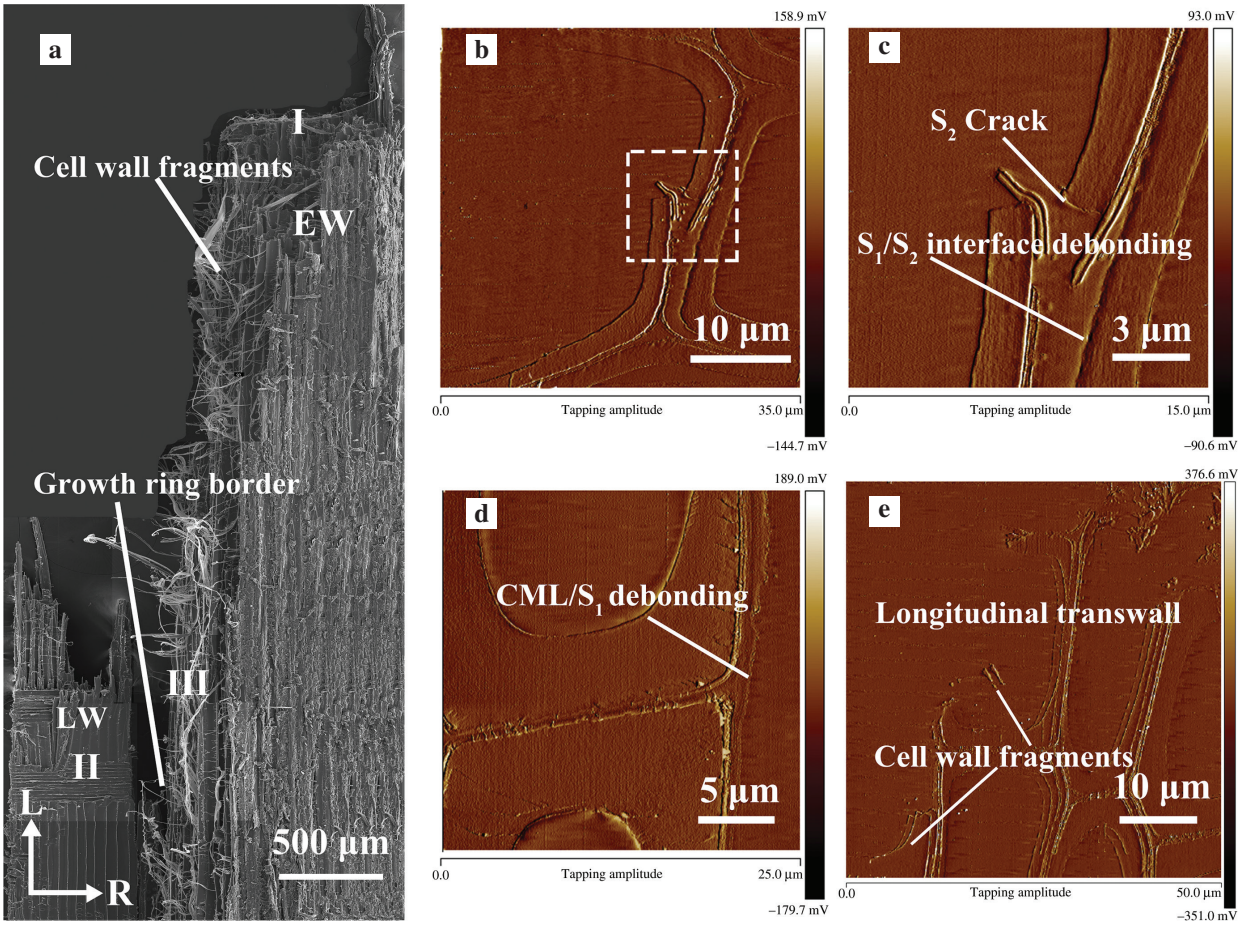

Figure 5: The fracture surface and tracheid cross-section fracture morphologies of the spruce EW/LW combination sample. (a) SEM image of the fracture surface; (b, d and e) AMF images of the tracheid cross-sections of the fracture regions I, II and III in Figure 5a, respectively; (c) enlarged version of the section within the dashed lines in b.

Additionally, the resin duct in the Masson pine led to crack propagation a long distance along the longitudinal direction compared with the spruce EW/LW fracture sample (Figures 5a and 6a).

The effects of softwood structure differences on the fracture behavior

EW and LW

The load-displacement curves are presented in Figures 7 and 8. The strain differences between the EW and LW in regard to wood deformation were monitored by tracking the displacement of markers on the specimen surface. A series of longitudinal and transverse strains mapping images corresponding to the various stages of loading as indicated by points A–D on the load-displacement curves are also presented in Figures 7 and 8. The changes in longitudinal and transverse strains between the EW and LW at different loading times are shown in Figure 9. For the spruce EW/LW specimen, the tensile behaviors of the EW and LW in the first few seconds were not significantly different (Figure 9a). With the increase in longitudinal tensile displacement, the longitudinal strain of the EW was more than that of the LW (Figure 9a). Furthermore, the transverse strain of the EW spruce was negative, which indicated that the EW incurred transverse shrinkage, but the transverse strain of the LW was positive (Figures 7 and 9b). So the growth ring boundary became a mechanical sensitive interface. For the Masson pine EW/LW specimen, the tensile behaviors of EW and LW over 35 s were not significantly different (Figure 9c), but the longitudinal strain of the EW in the larger longitudinal tensile displacement was also more than that of the LW (Figure 9c). Furthermore, the transverse strains of the EW and LW were negative, but the EW transverse strain was more than that of the LW (Figures 8 and 9d).

The differences in longitudinal strain between two growth ring constituents led to shear stress and parallel-to-grain cracks at the growth ring border. Furthermore, if

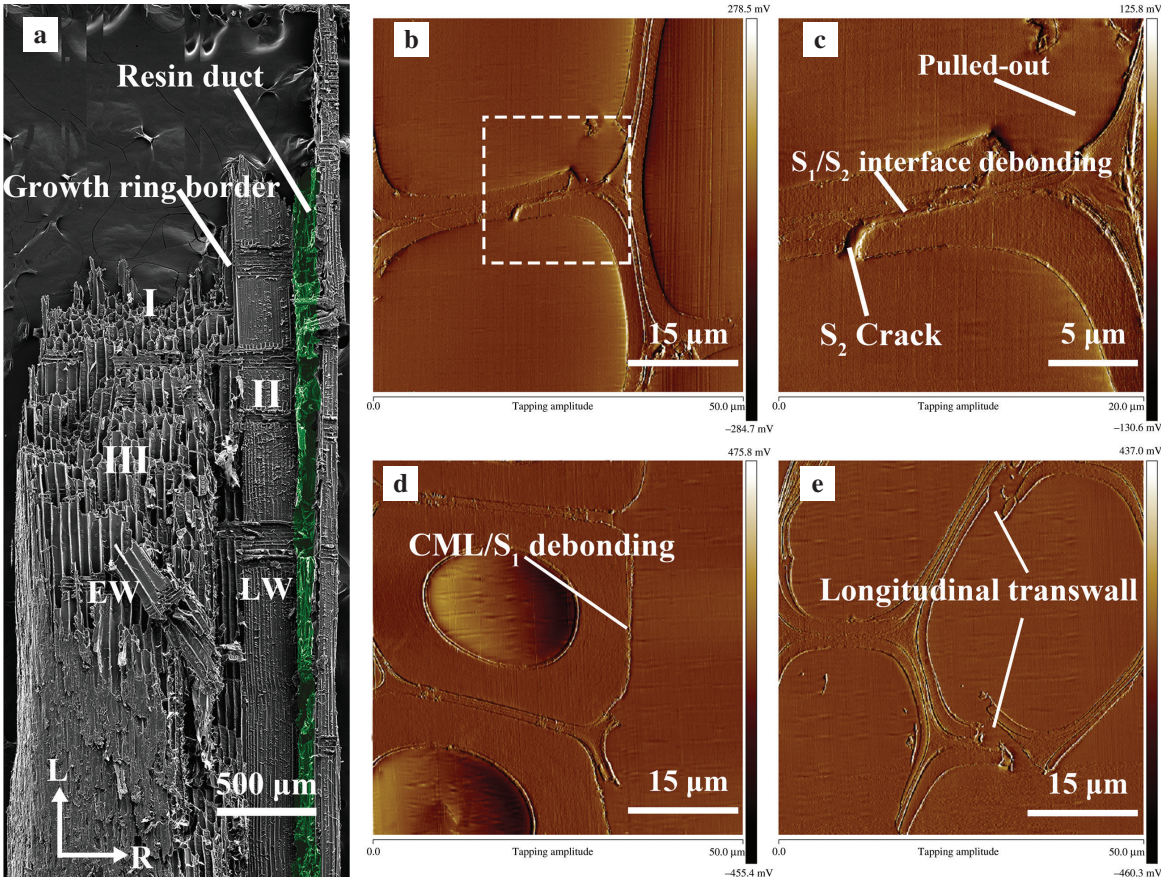

Figure 6: The fracture surface and tracheid cross-section fracture morphologies of the Masson pine EW/LW combination sample. (a) SEM image of the fracture surface; (b, d and e) AMF images of the tracheid cross-sections of fracture regions I, II and III in Figure 5a, respectively; (c) enlarged version of the section within the dashed lines in b.

a single tracheid is stressed, it collapses inward, thereby decreasing its diameter and allowing further elongation (Jeronimidis 1976). However, in a bulk specimen, tracheids firmly adhere to each other and are not able to collapse individually. Most likely, therefore, these deformation forces are transformed into transverse tensile strains, which accumulate and lead to the formation of parallel-to-grain cracks. The differences in transverse strains between the EW and LW might also lead to cracks mainly developing at the growth ring border (Farruggia and Perré 2000). So the shear stress caused the crack to propagate along the wood grain in the growth ring boundary, and in the EW of the growth ring boundary to cause longitudinal transwall breakage.

Wood rays

The effect of wood rays on the longitudinal strain maps of the Masson pine EW/LW combination sample is schematized in Figure 8. The strain concentration of the sample occurred in the wood ray portion of the EW (Figure 8). From a mechanical point of view, wood rays are weak spots, and the cracks in the EW have been associated with wood rays and heavily pitted areas (Bodner et al. 1996, 1997). The main reason for this occurrence is that the region between the tracheids and wood rays had significant pits, which lead to stress concentration at the pit edge positions of the tracheids or wood rays (Bodner et al. 1996, 1997). Our observations, presented in Figure 8, support this view; furthermore, it is believed that the initial crack might also occur in this strain concentration region. So wood rays, whether in EW or LW tissues, easily caused the crack to grow along the radial direction and promoted transverse transwall breakage of the tracheids (Figure 6).

Cell wall structure

The effects of the relative contents of a wood's components and microfibril angle (MFA) in the tracheid wall

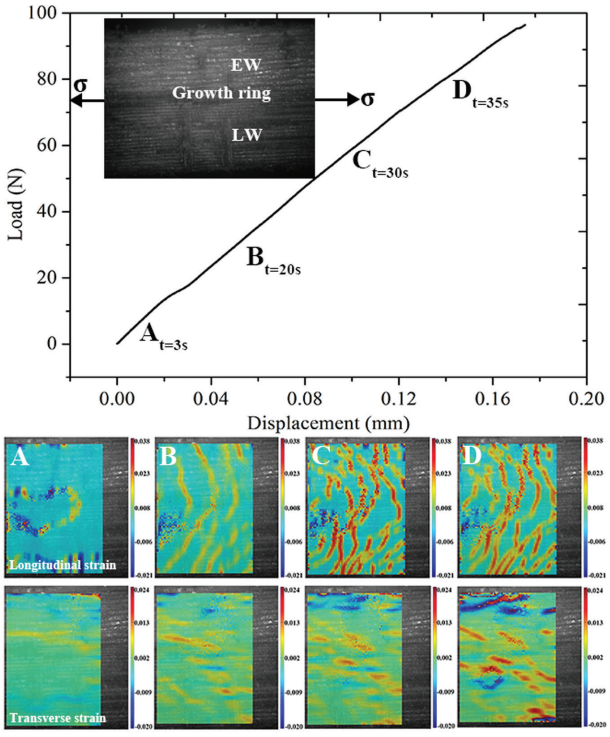

Figure 7: Typical load-displacement curve of the spruce EW/LW combination sample, and the longitudinal and transverse strains field images corresponding to the various loading stages as indicated by points A–D on the load-displacement curve.

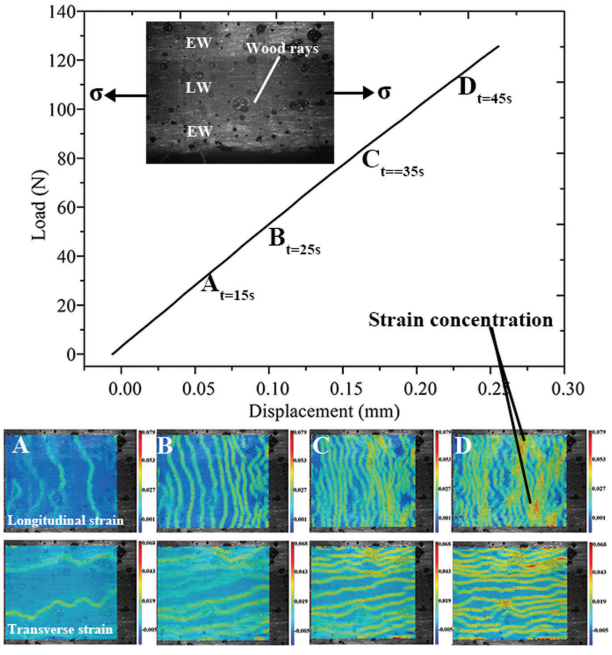

Figure 8: Typical load-displacement curve of the Masson pine EW/LW combination sample, and the longitudinal and transverse strains field images corresponding to the various loading stages as indicated by points A–D on the load-displacement curve.

on cell wall fracturing are significant. The higher level of lignin concentration in the ML layer (Donaldson 1995; Schmidt et al. 2009; Ji et al. 2014; Wang et al. 2014) and the relatively high content of pectin and protein in the primary wall (Stevanic and Salmén 2008) indicate that the CML layer could have an exceptional deformation capability compared to the secondary wall. As a stress transmitter and weak interface, it allows the adjacent secondary wall to incur a greater shear slip when the wood is stretched along the longitudinal direction. Hence, cell wall failure under longitudinal tensile load only occurred in the secondary cell wall rather than in the CML, a conclusion also earlier widely confirmed (Mark 1967).

The main difference between the three layers of the tracheid secondary wall is the MFA (α) (Funada and Abe 2005). Figure 10 shows the deformation mechanism of the cell wall under longitudinal tensile load. The longitudinal tensile deformations of the cell wall layer mainly include deformation of shear slip between the matrix and cellulose (Weinkamer and Fratzl, 2011) and the deformations of cellulose extension (ε_F) and matrix (ε_M) (Šturcová et al. 2006; Salmén and Bergström, 2009). Furthermore, with an increasing arrangement angle, the stress component (σ_M) perpendicular to the fiber direction increases, but the stress component (σ_F) parallel to the fiber direction decreases. So the maximum longitudinal strain and extensibility of the cell wall increased as the MFA increased (Reiterer et al. 2001; Adler and Buehler 2013). For the S_1 or S_3 layers with larger MFA, the larger stress component perpendicular to the cellulose chain length direction leads to increase in matrix deformation. So the deformation capability of the S_1 or S_3 was more than that of the S_2 layer, which led to stress redistribution and concentration occurring in the S_2 layer. Furthermore, the brittle behavior of the lignin and the induced shear stresses will cause shear failures between the microfibrils in the S_2 layer (Jeronimidis 1980). Therefore, the transverse transwall breakage type of the tracheids under longitudinal tension stress led to the fracture of the S_2 layer and the formation of the trumpet-shaped cracks (Figures 3 and 4). Finally, the initial trumpet-shaped fracture in the S_2 layer propagated into the S_1/S_2 interface (Figures 3 and 4). The main reason for this occurrence was that the S_1 layer of the larger MFA could force the initial crack to propagate along the interface with its lower crack propagation resistance.

When the crack propagated along the wood grain in the EW tissue, this resulted in the EW longitudinal transwall breakage type, and the cell lumen was completely exposed. This may be related to the low thickness of the EW wall; however, the crack propagated along the wood

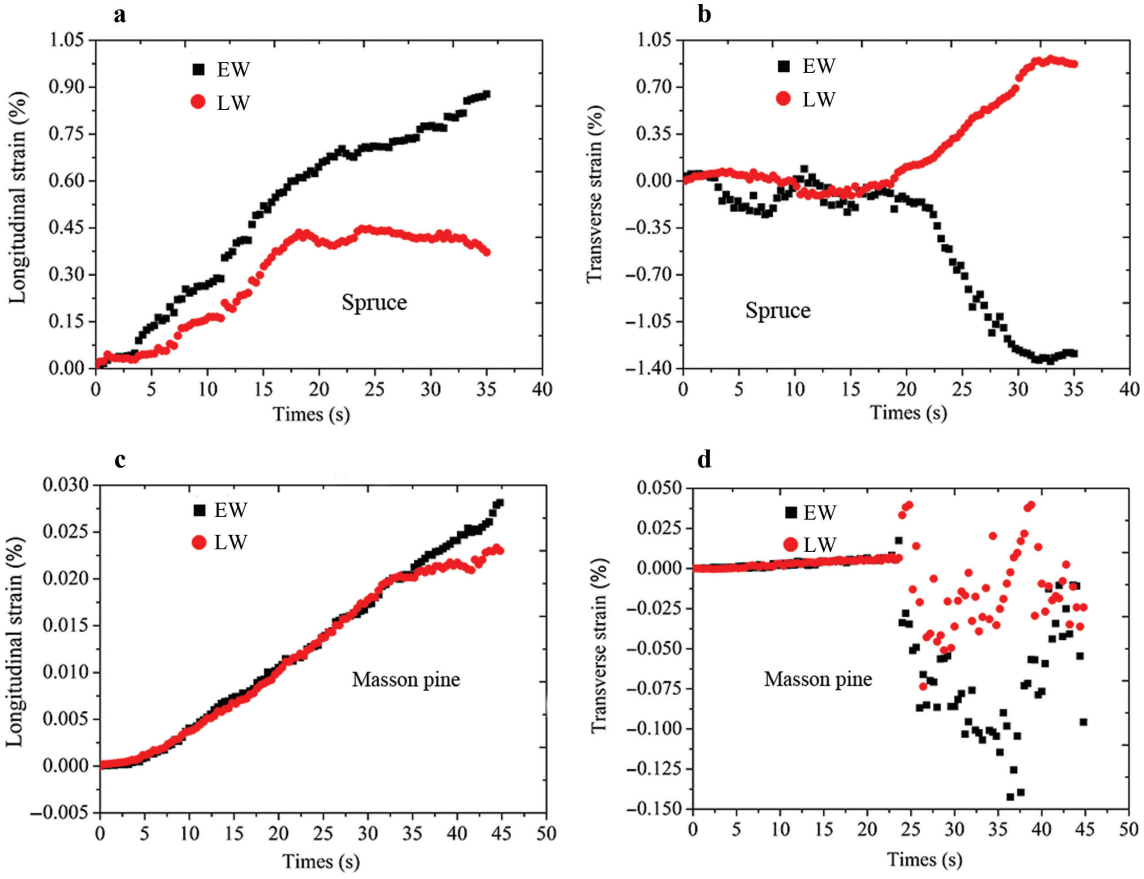

Figure 9: The longitudinal and transverse strains of the EW/LW combination samples of spruce and Masson pine.
(a) Longitudinal strain of spruce EW and LW; (b) transverse strain of spruce EW and LW; (c) longitudinal strain of Masson pine EW and LW; (d) transverse strain of Masson pine EW and LW.

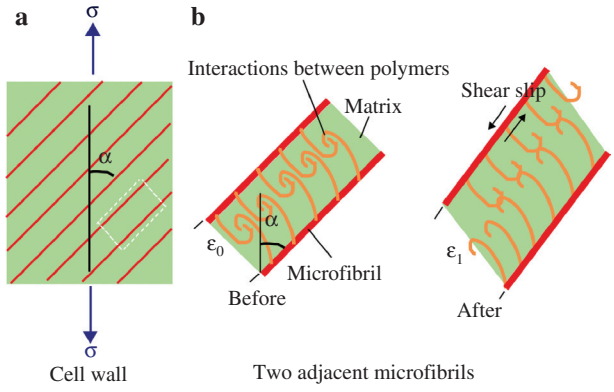

Figure 10: The deformation mechanism of the cell wall under longitudinal tensile load.
(a) Schematic deformation mechanism of the cell wall. (b) Enlarged version of the area within the dashed lines in (a).

grain in the LW tissue, and the delamination predominantly occurred at the CML/S_1 interface region, likely owing to the high lignin content of the CML region.

Conclusions

The main tracheid fracture of the EW sample was transverse transwall breakage, and the tracheid fracture process of the transverse transwall breakage was initiated as a fracture in the S_2 layer, with the crack propagating into the S_1/S_2 interface. For the EW/LW sample, the strain concentration and initial crack under longitudinal tension generally occur in the wood rays in EW tissue, which caused tracheids to undergo transverse transwall breakage. The initial fracture also occurred in the S_2 layer, and the crack propagated into the S_1/S_2 interface. When the crack propagated along the wood grain in the EW tissue or growth ring boundary, this resulted in the EW longitudinal transwall breakage, and the cell lumen was completely exposed. However, cracks propagating along the wood grain in the LW tissue could cause the LW tracheid to experience intrawall breakage, with the crack occurring predominantly at the CML/S_1 interface region.

Author contributions: All the authors have accepted responsibility for the entire content of this submitted manuscript and approved submission.
Research funding: The authors gratefully acknowledge the financial support of the Nature Science Foundation of China (no. 31770597) and the program from the China Scholarship Council (no. 201803270009).
Employment or leadership: None declared.
Honorarium: None declared.

References

Adler, D.C., Buehler, M.J. (2013) Mesoscale mechanics of wood cell walls under axial strain. Soft Matter 9:7138–7144.
Akande, J.A., Kyanka, G.H. (1990) Evaluation of tensile fracture in aspen using fractographic and theoretical methods. Wood Fiber Sci. 22:283–297.
Bodner, J., Grüll, G., Schlag, M.G. (1996) In-situ fracturing of wood in the scanning electron microscope. Holzforschung 50:487–490.
Bodner, J., Schlag, M.G., Grüll, G. (1997) Fracture initiation and progress in wood specimens stressed in tension. Part I. Clear wood specimens stressed parallel to the grain. Holzforschung 51:479–484.
Bodner, J., Schlag, M.G., Grüll, G. (1998) Fracture initiation and progress in wood specimens stressed in tension. Part III. Clear wood specimens with various slopes of grain. Holzforschung 52:95–101.
Büyüksari, Ü., As, N., Dündar, T. (2017) Mechanical properties of earlywood and latewood sections of Scots pine wood. Bioresources 12:4004–4012.
Cramer, S., Kretschmann, D., Lakes, R., Schmidt, T. (2005) Earlywood and latewood elastic properties in loblolly pine. Holzforschung 59:531–538.
Cote, W.A., Hanna, R.B. (1983) Ultrasound characteristics of wood fracture surfaces. Wood Fiber Sci. 15:135–163.
Davies, G.W. (1968) Microscopic observations of wood fracture. Holzforschung 22:177–180.
Donaldson, L.A. (1995) Cell wall fracture properties in relation to lignin distribution and cell dimensions among three genetic groups of radiata pine. Wood Sci. Technol. 29:51–63.
Farruggia, F., Perré, P. (2000) Microscopic tensile tests in the transverse plane of earlywood and latewood parts of spruce. Wood Sci. Technol. 34:65–82.
Fahlén, J., Salmén, L. (2002) On the lamellar structure of the tracheid cell wall. Plant Biol. 4:339–345.
Funada, R., Abe, H. (2005) Review – the orientation of cellulose microfibrils in the cell walls of tracheids in conifers. IAWA J. 26:161–174.
Jeronimidis, G. (1976) Fracture of wood in relation to its structure. Leiden Bot. Ser. 3:253–265.
Jeronimidis, G. (1980) The fracture behaviour of wood and the relations between toughness and morphology. Proc R Soc Lond. Ser B: Biol. Sci. 208:447–460.
Ji, Z., Ma, J., Xu, F. (2014) Multi-scale visualization of dynamic changes in poplar cell walls during alkali pretreatment. Microsc. Microanal. 20:566–576.
Koran, Z. (1968) Electron microscopy of tangential tracheid surfaces of black spruce produced by tensile failure at various temperatures. Svensk Papperstidning 71:567–576.
Lanvermann, C., Hass, P., Wittel, F.K., Niemz, P. (2014) Mechanical properties of Norway spruce: intra-ring variation and generic behavior of earlywood and latewood until failure. BioResources 9:105–119.
Lukacevic, M., Füssl, J., Lampert, R. (2015) Fracture mechanisms of clear wood identified at wood cell level by an approach based on the extended finite element method. Eng. Fract. Mech. 144:158–175.
Mark, R.E. (1967) Cell wall mechanics of tracheids. In: Tests of Mechanical Properties. Ed. Mark, R.E. Yale University Press, New Haven and London. pp. 27–53.
Mott, L., Shaler, S.M., Groom, L.H., Liang, B.H. (1995) The tensile testing of individual wood fibers using environmental scanning electron microscopy and video image analysis. TAPPI J. 78:143–148.
Reiterer, A., Lichtenegger, H., Fratzl, P., Stanzl-Tschegg, S.E. (2001) Deformation and energy absorption of wood cell walls with different nanostructure under tensile loading. J. Mater. Sci. 36:4681–4686.
Salmén, L., Bergström, E. (2009) Cellulose structural arrangement in relation to spectral changes in tensile loading FTIR. Cellulose 16:975–982.
Schmidt, M., Schwartzberg, A.M., Perera, P.N., Weber-Bargioni, A., Carroll, A., Sarkar, P., Capanema, E.A. (2009) Label-free in situ imaging of lignification in the cell wall of low lignin transgenic Populus trichocarpa. Planta. 230:589–597.
Sinn, G., Reiterer, A., Stanzl-Tschegg, S.E., Tschegg, E.K. (2001) Determination of strains of thin wood samples using videoextensometry. Eur. J. Wood Wood Prod. 59:177–182.
Sippola, M., Frühmann, K. (2002) In situ longitudinal tensile tests of pine wood in an environmental scanning electron microscope. Holzforschung 56:669–675.
Smith, I., Vasic, S. (2003) Fracture behaviour of softwood. Mech. Mater. 358:803–815.
Stanzl-Tschegg, S.E., Navi, P. (2009) Fracture behaviour of wood and its composites. A review. Holzforschung 63:139–149.
Stevanic, J.S., Salmén, L. (2008) Characterizing wood polymers in the primary cell wall of Norway spruce (Picea abies (L.) Karst.) using dynamic FT-IR spectroscopy. Cellulose 15:285–295.
Šturcová, A., Eichhorn, S.J., Jarvis, M.C. (2006) Vibrational spectroscopy of biopolymers under mechanical stress: processing cellulose spectra using bandshift difference integrals. Biomacromolecules 7:2688–2691.
Wang, X., Keplinger, T., Gierlinger, N., Burgert, I. (2014) Plant material features responsible for bamboo's excellent mechanical performance: a comparison of tensile properties of bamboo and spruce at the tissue, fibre and cell wall levels. Ann. Bot. Lond. 114:1627–1635.
Weinkamer, R., Fratzl, P. (2011) Mechanical adaptation of biological materials the examples of bone and wood. Mater. Sci. Eng. C 31:1164–1173.
Zink, A.G., Pellicane, P.J., Shuler, C.E. (1994) Ultrastructural analysis of softwood fracture surfaces. Wood Sci. Technol. 28:329–338.